https://dx.doi.org/10.1016/j.jcsr.2019.05.037
This is the Pre-Published Version.

The continuous strength method for the design of high strength steel tubular sections in bending

Xiaoyi Lan[a], Junbo Chen[a], Tak-Ming Chan[a,*], Ben Young[b]

[a] Dept. of Civil and Environmental Engineering, The Hong Kong Polytechnic University, Hong Kong, China

[b] Dept. of Civil and Environmental Engineering, The Hong Kong Polytechnic University, Hong Kong, China (Formerly, Dept. of Civil Engineering, The University of Hong Kong, Hong Kong, China)

*tak-ming.chan@polyu.edu.hk

Abstract: The continuous strength method (CSM) adopts base curves which relate the deformation capacity to its overall cross-section slenderness to take into account the element interaction and employs elastic, linear hardening material models to exploit the strength enhancement from strain hardening. This paper extends the CSM for structural design of hot-finished and cold-formed high strength steel tubular sections under bending. Results of 146 tests in the literature were compiled and a parametric study on 660 high strength steel tubular beams was conducted using validated finite element models. Base curves and resistance functions were proposed for non-slender and slender high strength steel circular hollow sections (CHS), elliptical hollow sections (EHS), square hollow sections (SHS) and rectangular hollow sections (RHS). Bi-linear and tri-linear material models were adopted for cold-formed and hot-finished steel tubular sections, respectively. Experimental and numerical results of 806 tubular beams were used to assess the proposed CSM, the direct strength method (DSM) and codified design methods. The resistance prediction of the proposed CSM is more accurate and less scattered.

Keywords: Continuous strength method; High strength steel; Moment resistance; Structural design; Tubular section

1. Introduction

The popularity of high strength steel (HSS) with yield stresses higher than 450 MPa is increasing. The application of HSS with high strength-to-weight ratio in tubular structures could reduce member sizes and structural self-weight, resulting in material savings, reduced costs of transportation, coatings and foundations and thus lower construction costs. Carbon footprints are also reduced because of less resource consumption and transportation time. Design rules for HSS tubular sections are needed to facilitate the structural application of HSS tubular structures.

The traditional effective width method defines the overall cross-section slenderness using the slenderest constituent plate within a cross-section, and consequently the plate element interaction cannot be considered. The effective width method is adopted by design codes and specifications including EN 1993-1-1 [1], EN 1993-1-5 [2], ANSI/AISC 360-10 [3] and AISI S100 [4]. Design rules based on shell buckling theory are also available for the design of shells in EN 1993-1-6 [5]. The strength-based direct strength method (DSM) [6, 7] adopts strength curves which relate the cross-section resistance to its overall cross-section slenderness for designing cold-formed structural steel members with flat elements. The DSM can therefore consider the element interaction and is currently adopted by AISI S100 [4] as an alternative design method. These codified design methods adopt an elastic, perfectly-plastic material model and consequently the strength enhancement from strain hardening is neglected. The deformation-based continuous strength method (CSM) proposed by Gardner and Nethercot [8], on the other hand, is for

© 2019. This manuscript version is made available under the CC-BY-NC-ND 4.0 license http://creativecommons.org/licenses/by-nc-nd/4.0/

designing non-slender stainless steel cross-section to rationally exploit the significant strain-hardening in stainless steel by adopting an elastic, linear hardening material model. Similar to the DSM, the CSM also employs base curves as a function of the overall cross-section slenderness to take into account the element interaction within cross-sections. To date, the CSM has been successfully extended for designing cross-sections using normal strength carbon steel [9-13], stainless steel [13-17], aluminium alloy [13, 18] and high strength steel [19]. The strength prediction of the CSM is demonstrated to be more accurate and consistent than that of the codified design methods. However, the proposed CSM by Lan et al. [19] is for designing HSS tubular sections subjected to axial compression, and research on the extension of the CSM to HSS tubular sections under bending remains limited.

This study extends the CSM for designing non-slender and slender HSS tubular sections subjected to bending. Current codified design methods and the CSM for designing steel cross-sections under bending were summarised. Results of 146 existing tests in the literature were compiled and a parametric study on 660 HSS tubular beams was conducted. Base curves and resistance functions were proposed for HSS CHS, EHS, SHS and RHS. The proposed CSM, the DSM and the codified design methods were assessed against results of existing tests in the literature and parametric study performed herein.

2. Codified design methods for carbon steel cross-sections

2.1. General

The concept of cross-section classification is adopted in EN 1993-1-1 [1], ANSI/AISC 360-10 [3] and AISI S100 [4] for designing carbon steel cross-sections under bending. Plastic and yield slenderness limits are stipulated to classify steel cross-sections. If the web and flange slenderness is smaller than the specified plastic slenderness limits, compact or Class 1-2 cross-sections are classified. Compact or Class 1-2 cross-sections can attain moment resistances at least the plastic moment capacity $M_{pl}=W_{pl}f_y$, where W_{pl} is the plastic section modulus and f_y is the steel yield stress. Cross-sections which can form a plastic hinge with sufficient rotation capacity for plastic design are classified as Class 1 cross-sections. Cross-sections with web and flange slenderness smaller than the yield slenderness limits but larger than the plastic slenderness limits are classified as non-compact or Class 3 cross-sections. The moment capacity of non-compact cross-sections is higher than the elastic moment capacity $M_{el}=W_{el}f_y$, where W_{el} is the elastic section modulus, but lower than the plastic moment capacity (M_{pl}). If the web or flange slenderness is larger than the yield slenderness limits, the cross-sections are slender or Class 4 cross-sections, and the corresponding moment resistances equal to the effective moment capacity $M_{eff}=W_{eff}f_y$, where W_{eff} is the effective section modulus. The direct strength method (DSM) adopts a strength curve as a function of its overall cross-section slenderness for designing cold-formed structural steel members and is currently incorporated in AISI S100 [4] as an alternative design method. It should be noted that the design of EHS is not covered in the design codes and specifications [1-5]. The current codified design methods for SHS, RHS and CHS are summarised in following subsections.

2.2. Design of square and rectangular hollow sections

EN 1993-1-1 [1] gives step-wise nominal strength prediction for SHS and RHS in bending, i.e. M_{pl} for Class 1-2, M_{el} for Class 3 and M_{eff} for Class 4 cross-sections. The effective section modulus (W_{eff}) of slender SHS and RHS can be obtained from EN 1993-1-5 [2]. In contrast, ANSI/AISC 360-10 [3] provides

continuous nominal strength prediction for SHS and RHS under bending. For compact cross-sections, the moment resistance equals to the plastic moment capacity (M_{pl}). A linear transition from M_{pl} to M_{el} is specified for non-compact cross-sections. The effective width method is used to obtain the effective section modulus for flange local buckling of slender cross-sections while the web local buckling is neglected. In AISI S100 [4], the nominal moment resistance of SHS and RHS is determined as the lower of initial of yielding strength (M_{el}) and local buckling strength (M_{eff}) which can be obtained using the effective width method. The DSM adopts a strength curve as a function of overall cross-section slenderness. The nominal moment resistance of SHS and RHS under bending (M_{DSM}) can be obtained:

$$M_{DSM} = \begin{cases} M_{el} & \text{for } \lambda_p \le 0.776 \\ \left(1 - \dfrac{0.15}{\lambda_p^{0.8}}\right)\dfrac{1}{\lambda_p^{0.8}} M_{el} & \text{for } \lambda_p > 0.776 \end{cases} \quad (1)$$

$$\lambda_p = \sqrt{M_{el} / M_{cr}} \quad (2)$$

where λ_p is the overall cross-section slenderness, M_{el} is the elastic moment capacity, M_{cr} is the elastic buckling moment which could be obtained from approximate equations or software such as CUFSM [20] and ABAQUS [21].

2.3. Design of circular hollow sections

Similar to the design approach for SHS and RHS, EN 1993-1-1 [1] stipulates noncontinuous nominal strength prediction for CHS under bending. The moment resistance of CHS is M_{pl} for Class 1-2 and M_{el} for Class 3. The moment capacity of Class 4 CHS can be obtained from EN 1993-1-6 [5] which adopts shell buckling theory as follows:

$$M_{EC3\text{-}1\text{-}6} = \pi r^2 t \chi f_y \quad (3)$$

where r is the radius of cylinder middle surface, t is the wall thickness, χ is the buckling reduction factor and f_y is the steel yield stress. The nominal moment resistance given in ANSI/AISC 360-10 [3] for CHS is as follows:

$$M_{AISC} = \begin{cases} M_{pl} & \text{for } \lambda \le 0.07 \\ (1 + 0.021/\lambda) M_{el} & \text{for } 0.07 < \lambda \le 0.31 \\ 0.33 M_{el} / \lambda & \text{for } 0.31 < \lambda \le 0.45 \end{cases} \quad (4)$$

where λ is the cross-section slenderness and equals to $(D/t)(f_y/E)$, D is the outer diameter of CHS, t is the wall thickness, f_y is the steel yield stress and E is the elastic modulus. Similar nominal strength equation is specified in AISI S100 [4] for CHS as follows:

$$M_{AISI} = \begin{cases} 1.25 M_{el} & \text{for } \lambda \le 0.0714 \\ (0.97 + 0.02/\lambda) M_{el} & \text{for } 0.0714 < \lambda \le 0.318 \\ 0.328 M_{el} / \lambda & \text{for } 0.318 < \lambda \le 0.441 \end{cases} \quad (5)$$

The DSM is originally proposed for designing cold-formed steel members with flat elements. Lan et al. [19] found that the DSM yield slenderness limit (λ_p=0.776) and strength equation are not applicable for high strength steel CHS and EHS under compression. The suitability of the DSM for high strength steel CHS and EHS in bending needs to be examined.

3. The continuous strength method

3.1. General

The deformation-based CSM composes of two main components, i.e. the base curve and the elastic, linear hardening material model. The base curve defines the maximum attainable strain (ε_{csm}) normalised by the yield strain (ε_y) as a function of the overall cross-section slenderness (λ_p) given in Eq. (2), and thus the plate element interaction within cross-sections can be considered. The adopted elastic, linear hardening material model instead of elastic, perfectly-plastic material model used by codified design methods [1-5] is capable of rationally exploiting the strength enhancement from strain hardening. The following subsections describe the current CSM for designing steel cross-sections under bending.

3.2. Base curve

The CSM base curve relates the maximum attainable strain (ε_{csm}) divided by the yield strain (ε_y) to the overall cross-section slenderness (λ_p). The base curves proposed for non-slender and slender cross-section using stainless steel and aluminium alloy [17, 18] under bending are as follows:

$$\frac{\varepsilon_{csm}}{\varepsilon_y} = \frac{k_u y_{max} - 0.002}{k_{el} y_{max}} = \frac{0.25}{\lambda_p^{3.6}} \leq \min\left(15, \frac{C_1 \varepsilon_u}{\varepsilon_y}\right) \quad \text{for} \quad \lambda_p \leq 0.68 \tag{6}$$

$$\frac{\varepsilon_{csm}}{\varepsilon_y} = \frac{M_u}{M_{el}} = \left(1 - \frac{0.222}{\lambda_p^{1.05}}\right)\frac{1}{\lambda_p^{1.05}} \quad \text{for} \quad \lambda_p > 0.68 \tag{7}$$

where ε_{csm} is the CSM limiting strain, ε_y is the yield strain which equals to f_y/E, k_u and k_{el} are the curvatures at the ultimate load and the elastic moment capacity, respectively, y_{max} is the distance from the elastic neutral axis to the extreme fibre of the cross-section, C_1 is the coefficient defining a cut-off strain to avoid over-prediction of material stress, M_u is the experimental or numerical ultimate moment of beams, M_{el} is the elastic moment capacity of cross-sections. The CSM limiting strain (ε_{csm}) equals to $\varepsilon_{csm}=k_u y_{max}-0.002$ for non-slender cross-sections with a round material response (e.g. stainless steel and aluminium alloy), and $\varepsilon_{csm}= k_u y_{max}$ for those with a sharply defined yield point (e.g. hot-finished steel) to be compatible with the CSM material models described in Section 3.3. Two upper bounds of 15 and $C_1\varepsilon_u/\varepsilon_y$ are imposed on the normalised cross-section deformation capacity ($\varepsilon_{csm}/\varepsilon_y$). The first limit of 15 is to be in line with the material ductility requirement in EN 1993-1-1 [1] and avoids excessive plastic strain, and the second limit of $C_1\varepsilon_u/\varepsilon_y$ prevents over-prediction of material strengths. It should be noted that Eq. (6) was also adopted for designing non-slender normal strength carbon steel cross-sections at room and elevated temperatures [9-12], and the proposed base curves defined by Eqs. (6-7) are for designing cross-sections with flat plate elements e.g. SHS, RHS and I-sections. Lan et al. [19] proposed base curves for designing non-slender and slender high strength steel SHS and RHS in compression as follows:

$$\frac{\varepsilon_{csm}}{\varepsilon_y} = \frac{0.294}{\lambda_p^{3.174}} \leq \min\left(15, \frac{C_1 \varepsilon_u}{\varepsilon_y}\right) \quad \text{for} \quad \lambda_p \leq 0.68 \tag{8}$$

$$\frac{\varepsilon_{csm}}{\varepsilon_y}=\left(1-\frac{0.219}{\lambda_p^{1.014}}\right)\frac{1}{\lambda_p^{1.014}} \qquad \text{for} \quad 0.68<\lambda_p\le 2.61 \tag{9}$$

150 The base curves defined by Eqs. (6-9) are not applicable for the design of CHS as the slenderness limit of
151 0.68 is not suitable for CHS. Buchanan et al. [13] proposed base curves for CHS using stainless steel,
152 aluminium alloy and normal strength carbon steel as follows:

$$\frac{\varepsilon_{csm}}{\varepsilon_y}=\frac{4.44\times10^{-3}}{\lambda_p^{4.5}}\le\min\left(15,\frac{C_1\varepsilon_u}{\varepsilon_y}\right) \qquad \text{for} \quad \lambda_p\le 0.3 \tag{10}$$

$$\frac{\varepsilon_{csm}}{\varepsilon_y}=\left(1-\frac{0.224}{\lambda_p^{0.342}}\right)\frac{1}{\lambda_p^{0.342}} \qquad \text{for} \quad 0.3<\lambda_p\le 0.6 \tag{11}$$

153 Lan et al. [19] found that the slenderness limit of 0.3 is conservative for designing high strength steel CHS,
154 and proposed base curves for high strength steel CHS and EHS under compression as follows:

$$\frac{\varepsilon_{csm}}{\varepsilon_y}=\frac{0.015}{\lambda_p^{4.0}}\le\min\left(15,\frac{C_1\varepsilon_u}{\varepsilon_y}\right) \qquad \text{for} \quad \lambda_p\le 0.35 \tag{12}$$

$$\frac{\varepsilon_{csm}}{\varepsilon_y}=\left(1-\frac{0.223}{\lambda_p^{0.44}}\right)\frac{1}{\lambda_p^{0.44}} \qquad \text{for} \quad 0.35<\lambda_p\le 0.90 \tag{13}$$

155

156 *3.3. Material models*

157

158 Elastic, linear strain hardening material models are adopted in the CSM design framework to rationally
159 exploit the capacity enhancement from strain hardening. A bi-linear material model is employed for steel
160 cross-sections with a round material response, and the CSM limiting stress (f_{csm}) is obtained from [10-19]:

$$f_{csm}=\begin{cases}E\varepsilon_{csm} & \text{for } \varepsilon_{csm}\le\varepsilon_y\\ f_y+E_{sh}\left(\varepsilon_{csm}-\varepsilon_y\right) & \text{for } \varepsilon_{csm}>\varepsilon_y\end{cases} \tag{14}$$

$$E_{sh}=\frac{f_u-f_y}{C_2\varepsilon_u-\varepsilon_y} \tag{15}$$

$$\varepsilon_u=C_3\left(1-f_y/f_u\right)+C_4 \tag{16}$$

161 where E is the elastic modulus, E_{sh} is the strain-hardening modulus, ε_{csm} is the CSM limiting strain, ε_y is
162 the yield strain, ε_u is the ultimate strain at ultimate stress, f_y is the yield stress, f_u is the ultimate stress and
163 C_2 is the coefficient for the determination of strain hardening slope. Table 1 summarises the values of C_1,
164 C_2, C_3 and C_4 reported in Buchanan et al. [13] for different types of steel.
165 The bi-linear material model is less suitable for steel materials with a sharply defined yield point
166 because of the existence of a yield plateau. A tri-linear material model originally from the quad-linear
167 material model for hot-rolled steel proposed by Yun and Gardner [22] is adopted for steel materials with a
168 sharply defined yield point, and the CSM limiting stress (f_{csm}) can be determined from [9, 19]:

$$f_{csm} = \begin{cases} E\varepsilon_{csm} & \text{for } \varepsilon_{csm} \le \varepsilon_y \\ f_y & \text{for } \varepsilon_y < \varepsilon_{csm} \le \varepsilon_{sh} \\ f_y + E_{sh}(\varepsilon_{csm} - \varepsilon_{sh}) & \text{for } \varepsilon_{sh} < \varepsilon_{csm} \le C_1\varepsilon_u \end{cases} \quad (17)$$

$$C_1 = \frac{\varepsilon_{sh} + 0.25(\varepsilon_u - \varepsilon_{sh})}{\varepsilon_u} \quad (18)$$

$$\varepsilon_{sh} = 0.1 f_y / f_u - 0.055 \quad \text{but } 0.015 \le \varepsilon_{sh} \le 0.03 \quad (19)$$

$$\varepsilon_u = 0.6(1 - f_y / f_u) \quad \text{but } \varepsilon_u \ge 0.06 \quad (20)$$

$$E_{sh} = \frac{f_u - f_y}{0.4(\varepsilon_u - \varepsilon_{sh})} \quad (21)$$

where C_1 is the material coefficient and ε_{sh} is the strain-hardening strain.

3.4. Cross-section resistance

The CSM moment resistance (M_{csm}) of SHS, RHS and CHS with a round material response may be determined from [11-18]:

$$M_{csm} = M_{pl}\left[1 + \frac{E_{sh}}{E}\frac{W_{el}}{W_{pl}}\left(\frac{\varepsilon_{csm}}{\varepsilon_y} - 1\right) - \left(1 - \frac{W_{el}}{W_{pl}}\right)\Big/\left(\frac{\varepsilon_{csm}}{\varepsilon_y}\right)^2\right] \quad \text{for } \varepsilon_{csm} > \varepsilon_y \quad (22)$$

$$M_{csm} = \frac{\varepsilon_{csm}}{\varepsilon_y} M_{el} \quad \text{for } \varepsilon_{csm} \le \varepsilon_y \quad (23)$$

For steel materials with a distinctive yield plateau, the CSM moment capacity of slender RHS and SHS can be calculated from Eq. (23), and the CSM moment resistance of non-slender RHS and SHS may be approximated by [9]:

$$M_{csm} = M_{pl}\left[1 - \left(1 - \frac{W_{el}}{W_{pl}}\right)\Big/\left(\frac{\varepsilon_{csm}}{\varepsilon_y}\right)^2\right] \quad \text{for } \varepsilon_y < \varepsilon_{csm} \le \varepsilon_{sh} \quad (24)$$

$$M_{csm} = M_{pl}\left[1 - \left(1 - \frac{W_{el}}{W_{pl}}\right)\Big/\left(\frac{\varepsilon_{csm}}{\varepsilon_y}\right)^2 + 0.1\left(\frac{\varepsilon_{csm} - \varepsilon_{sh}}{\varepsilon_y}\right)^2 \frac{E_{sh}}{E}\right] \quad \text{for } \varepsilon_{csm} > \varepsilon_{sh} \quad (25)$$

4. Summary of experimental tests on tubular beams

Results of a total of 146 experimental tests on tubular beams which failed by cross-section yielding or local buckling were compiled including 65 CHS [23-28], 10 EHS [29], and 71 SHS and RHS [28, 30-31]. The measured yield stress (f_y), fabrication method, overall cross-section slenderness (λ_p) and number of tests in each experimental project are summarised in Tables 2-4. The ranges of overall cross-section slenderness (λ_p) in existing tests on tubular beams [23-31] are $0.15 \le \lambda_p \le 0.52$ for CHS, $0.18 \le \lambda_p \le 0.56$ for EHS and $0.16 \le \lambda_p \le 1.01$ for SHS and RHS. Most of CHS, SHS and RHS beams summarised in Tables 2 and

4 are in high strength steel. However, there is a lack of experimental tests on high strength steel EHS beams in the literature and therefore only test data of normal strength steel counterparts were collated as shown in Table 3. Tables 2-4 show that tests on the high strength steel tubular beams are limited. In order to supplement the limited test results, extensive finite element simulations were carried out as presented in Section 5.

5. Numerical modelling

5.1. General

The software ABAQUS version 6.13 [21] was used to carry out finite element (FE) analysis on structural responses of CHS, EHS, SHS and RHS beams under bending. FE models were validated against test results in Ma et al. [28] and Chan and Gardner [29], and then extensive numerical simulations were performed to extend ranges of cross-section geometries and slenderness. Tables 5-7 show key parameters of tubular beam specimens in tests [28-29] used for validating FE models including the outer diameter of CHS (D), larger outer diameter ($2a$) and smaller outer diameter ($2b$) of EHS, overall section height (H) and overall section width (B) of SHS and RHS, wall thickness (t), maximum imperfection (ω_0), steel yield stress (f_y) of CHS and EHS, and steel yield stress of flat portions (f_{yf}) and corner regions (f_{yc}) of cold-formed SHS and RHS.

Beam models under pure bending moment instead of full span models were developed and adopted in this study because the moment span models can provide accurate prediction of the structural behaviour of tubular beams in four-point bending tests and substantially reduce computational costs [9, 32]. The measured material properties were adopted for the validation of FE models. The value of Poisson's ratio (v) for steel materials was taken as 0.3. True stress-logarithmic plastic strain curves converted from engineering stress-strain curves were input into the FE models. The cold-forming effect of SHS and RHS beams was taken into account by assigning material properties of corner portions to the extended corner regions up to $2t$ [19]. The shell element i.e. S4R in ABAQUS was adopted in all FE models. The mesh sizes were carefully determined by a mesh sensitivity study. Mesh sizes of one twentieth of the average cross-section dimensions were employed, i.e. $D/20$ for CHS, $(2a+2b)/40$ for EHS and $(H+B)/40$ for SHS/RHS. The residual stress was not considered in the FE modelling because its effect on structural responses of tubular beams is insignificant [32]. The initial geometric imperfections of tubular beams were incorporated into the FE models using the lowest elastic buckling mode shape obtained from elastic eigenvalue analysis. The measured maximum imperfections (ω_0) listed in Tables 5-7 were taken as the amplitudes of the buckling mode in the validation study. The boundary conditions of moment span models were carefully chosen to closely simulate the test set-ups in four-point bending tests. The degrees of freedom of all nodes at each beam end were firstly coupled to a concentric reference point through rigid body constraints. All degrees of freedom of the reference points were then restricted expect the longitudinal translation at one end and rotation in the directions of major and minor bending at two ends. Fig. 1 shows corresponding boundary conditions adopted in the pure bending model. The bending moment was applied at the reference points by means of rotation in increments using the "Static" method, and the effect of geometric nonlinearity was taken into account using the parameter (*NLGEOM). The von-Mises yield criterion was adopted in FE analysis.

5.2. Validation of FE models

The failure modes, moment-curvature curves and ultimate resistances predicted by the numerical simulations were compared with those from experimental tests to validate the adopted FE models. Fig. 2 shows failure modes of CHS and SHS beams observed in tests and FE simulations. The failure modes predicted are shown to closely mirror test observations. It should be noted that the observed failure mode of EHS beams under four-point bending in tests was not shown in Chan and Gardner [29] and thus the corresponding comparison is not made. The comparison of moment-curvature curves of representative tubular beams is shown in Fig. 3. The FE models were found to provide accurate prediction of moment-curvature curves. Tables 5-7 summarise ultimate capacities obtained from finite element analysis (M_{FE}) and tests (M_u), and the corresponding curvatures at the ultimate resistance determined from numerical simulations (k_{FE}) and tests (k_u). The mean values of M_{FE}/M_u for CHS, EHS and SHS/RHS beams are 0.99, 1.02 and 1.03, respectively with corresponding COV of 0.01, 0.05 and 0.05. The mean values of k_{FE}/k_u for CHS, EHS and SHS/RHS beams are 0.96, 1.20 and 0.94, respectively with corresponding COV of 0.07, 0.10 and 0.09. It is shown that the predicted ultimate resistances and corresponding curvatures agree well with the test results. It is, therefore, concluded that the adopted FE models can produce accurate prediction of failure modes, moment-curvature curves, ultimate capacities and corresponding curvatures of tubular beams and are suitable for the subsequent numerical parametric study.

5.3. Parametric study

The developed FE models were adopted to carry out a parametric study on totally 660 high strength steel tubular beams of CHS, EHS and SHS/RHS. The parameters of tubular beams subjected to major and minor bending are summarised in Table 8. The cross-section type of tubular beams is represented by five letters with the first three letters denoting the cross-section shape (CHS, EHS, SHS and RHS) and the last two letters (HF or CF) indicating the steel type (hot-finished or cold-formed). Hot-finished steel grades S460, S550 and S690 and cold-formed steel grades S700, S900 and S1100 were included. This study employs the material parameters for hot-finished steel adopted by Lan et al. [19] and cold-formed steel proposed by Ma et al. [33]. The adopted material properties are summarised in Tables 9-10 including the elastic modulus (E), yield stress (f_y), and ultimate stress (f_u) and ultimate strain at ultimate stress (ε_u). The bi-linear plus nonlinear hardening material model for hot-rolled steel [22] and stress-strain curve models proposed by Ma et al. [33] for cold-formed steel were used herein. The external radius of SHS and RHS was taken in accordance with EN 10210-2 [34] and EN 10219-2 [35], i.e. 1.5t for hot-finished steel, and 2t, 2.5t and 3t for $t\leq6$, $6<t\leq10$ and $10<t$, respectively, for cold-formed steel. The lengths (L) of moment span models of CHS, EHS and SHS/RHS equal to 3D, 6a and 3H, respectively. The imperfection amplitude (ω_0) of CHS and EHS were obtained from Eq. (26), where Q equals to 40 for Class A fabrication quality, t is the wall thickness, r is the radius of middle surface for CHS and taken as the equivalent radius (i.e. a^2/b) for EHS [19].

$$\omega_0 = \frac{t}{Q}\sqrt{\frac{r}{t}} \tag{26}$$

Maximum out-of-flatness tolerances of 1.0%H and 0.8%H with a minimum value of 0.5 mm specified in EN 10210-2 [34] and EN 10219-2 [35] were taken as the imperfection amplitudes for hot-finished and cold-formed SHS/RHS, respectively. The adopted values of ω_0 are found to provide upper bounds of the measured maximum imperfections in tests described in Section 4, and thus can reasonably approximate the

level of imperfection amplitudes. The ranges of overall cross-section slenderness (λ_p) in the parametric study are $0.14 \le \lambda_p \le 0.76$ for CHS, $0.14 \le \lambda_p \le 0.85$ for EHS and $0.18 \le \lambda_p \le 2.14$ for SHS and RHS.

6. Extension of the CSM to high strength steel tubular sections

6.1. Base curves and material models

The CSM was extended for designing non-slender and slender high strength steel CHS, EHS, SHS and RHS in bending using the results of tests compiled in Section 4 and finite element simulations described in Section 5. Fig. 4 shows the test and FE results of tubular beams where the ultimate moment capacity (M_u) normalised by elastic moment capacity (M_{el}) is plotted against the overall cross-section slenderness (λ_p). It is shown that the limiting cross-section slenderness classifying non-slender and slender cross-sections is λ_p=0.50 for CHS and EHS which is comparable to the current yield slenderness limit adopted by ANSI/AISC 360-10 [3] for CHS. The limiting cross-section slenderness for SHS and RHS is λ_p=0.776 which is also employed by the current DSM (see Eq. (1)). The limiting cross-section slenderness proposed by Lan et al. [19] for high strength steel tubular sections in compression (i.e. λ_p=0.35 for CHS and EHS, and λ_p=0.68 for SHS and RHS) is conservative for the high strength steel CHS, EHS, SHS and RHS subjected to bending mainly because of the stress gradient in bending. The portions in lower stresses could provide restraints to those in higher stresses when compared with the tubular sections in uniform compression. It should be noted that the values of λ_p were determined by Eq. (2) and the elastic buckling moment (M_{cr}) was obtained using ABAQUS [21] in this study. The weighted average (by area) material properties were used for cold-formed SHS and RHS to take into account the cold-forming effect.

The maximum attainable strain (ε_{csm}) normalised by the yield strain (ε_y) collated from existing tests and obtained from numerical analysis against the overall cross-section slenderness (λ_p) is plotted in Figs. 5-6. The values of ε_{csm} were determined in accordance with current CSM as described in Section 3.2. Base curves for non-slender and slender high strength steel tubular sections were proposed using regression analysis of test and FE data. Figs. 5-6 show the proposed base curves defined by Eqs. (27-28) for CHS and EHS, and those defined by Eqs. (29-30) for SHS and RHS. It is shown that the base curves can provide reasonably accurate prediction of the $\varepsilon_{csm}/\varepsilon_y$ values for high strength steel CHS, EHS, SHS and RHS in bending. It should be noted that the upper limits of the proposed base curves are 0.85 for CHS and EHS, and 2.14 for SHS and RHS which are the upper limits of numerical and test data in this study.

$$\frac{\varepsilon_{csm}}{\varepsilon_y} = \frac{0.16}{\lambda_p^{2.65}} \le \min\left(15, \frac{C_1\varepsilon_u}{\varepsilon_y}\right) \quad \text{for} \quad \lambda_p \le 0.50 \tag{27}$$

$$\frac{\varepsilon_{csm}}{\varepsilon_y} = \left(1 - \frac{0.23}{\lambda_p^{0.64}}\right)\frac{1}{\lambda_p^{0.64}} \quad \text{for} \quad 0.50 < \lambda_p \le 0.85 \tag{28}$$

$$\frac{\varepsilon_{csm}}{\varepsilon_y} = \frac{0.50}{\lambda_p^{2.74}} \le \min\left(15, \frac{C_1\varepsilon_u}{\varepsilon_y}\right) \quad \text{for} \quad \lambda_p \le 0.776 \tag{29}$$

$$\frac{\varepsilon_{csm}}{\varepsilon_y} = \left(1 - \frac{0.10}{\lambda_p^{0.47}}\right)\frac{1}{\lambda_p^{0.47}} \quad \text{for} \quad 0.776 < \lambda_p \le 2.14 \tag{30}$$

The material models described in Section 3.3 were employed. The bi-linear material model defined by

Eq. (14) and coefficients (C_1-C_4) for cold-formed steel in Table 1 were used for cold-formed steel tubular sections. The tri-linear material model (see Eq. (17)) was adopted for hot-finished steel tubular sections.

6.2. CSM cross-section capacities

The moment resistances of cold-formed and hot-finished steel SHS and RHS in bending were determined using Eqs. (22-25). The moment capacities of cold-formed CHS were calculated from Eqs. (22-23). For hot-finished steel CHS and EHS with $\varepsilon_{csm} \leq \varepsilon_y$, Eq. (23) was used to obtain corresponding moment resistances. However, there are no available equations of bending resistance for hot-finished steel CHS and EHS with $\varepsilon_{csm} > \varepsilon_y$ in the literature. It is possible to derive exact equations for the hot-finished steel CHS and EHS, however, the expressions would be lengthy and not suitable for practical use. It should be noted that Eqs. (22-25) are reasonably accurate approximations to the exact expressions for the convenience of use.

The finite strip method (FSM) [36] was used to overcome difficulties in deriving the analytical expressions and to obtain cross-section capacities of hot-finished steel CHS and EHS with $\varepsilon_{csm} > \varepsilon_y$. The procedures of calculating moment resistances of EHS bending about minor axis are illustrated as follows, which can also be used to determine the moment capacities of EHS bending about major axis and CHS. A fourth of an elliptical hollow section was used due to symmetry which can be discretised into n small strips with equal height of b/n as shown in Fig. 7. The equation for an ellipse with larger and smaller outer diameter of $2a$ and $2b$, respectively, is as follows:

$$\frac{Z^2}{a^2} + \frac{Y^2}{b^2} = 1 \tag{31}$$

For a given value of Y_i which is equal to y_i, the corresponding Z_i value can be determined using Eq. (31), and z_i values were obtained for $0 \leq y_i < b-t$ in a similar way using the equation of an ellipse with larger and smaller outer diameter of $2a-2t$ and $2b-2t$, respectively while $z_i=0$ for $b-t \leq y_i \leq b$. When the number of strips (n) is sufficiently large, the area (A_i) of the i_{th} quadrilateral strip may be approximated by:

$$A_i = \frac{Z_i - z_i + Z_{i-1} - z_{i-1}}{2} \frac{b}{n} \tag{32}$$

Assuming cross-sections of beams remain plane and perpendicular to neutral axis after bending, the strain at the i_{th} strip:

$$\varepsilon_i = \frac{\varepsilon_{csm} Y_i^*}{b} \tag{33}$$

where ε_{csm} is the CSM limiting strain obtained from the adopted CSM base curves, and Y_i^* is the distance of the strip centroid from the neutral axis of the cross-section in y direction and equals to $(Y_{i-1}+Y_i)/2$. The stress at the i_{th} strip (f_i) was determined by the tri-linear material model described in Section 3.3. The moment resistance of an elliptical hollow section bending about minor axis can be obtained from:

$$M_z = 4\int_A f_i Y_i^* \mathrm{d}A = 4\sum_{i=1}^{n} f_i A_i Y_i^* \tag{34}$$

Sufficient number of strips (n) is needed to represent the cross-sections, such that approximation errors can be reasonably minimised. A sensitivity study was conducted to determine suitable strip number. The value

of n was taken as 1000 in this study and the change of moment resistances resulted from increasing the strip number is within 0.1%. In order to further validate the accuracy of the adopted finite strip method (FSM), the moment resistances (M_u) normalised by the plastic moment capacity (M_{pl}) of a typical cold-formed CHS obtained from the FSM were compared with those calculated from Eq. (22) (see Fig. 8(a)). It is shown that the adopted FSM can provide accurate prediction of moment capacities when n = 1000.

The applicability of Eqs. (24-25) for non-slender hot-finished steel CHS and EHS with $\varepsilon_{csm}>\varepsilon_y$ was examined. Figs. 8(b-c) show that comparison of the moment resistances of typical hot-finished steel CHS and EHS obtained using the FSM with those calculated from Eqs. (24-25). It is shown that the CSM resistance functions are accurate for $1\leq\varepsilon_{csm}/\varepsilon_y\leq15$ while increasingly overpredict the moment capacities when $\varepsilon_{csm}/\varepsilon_y>15$. It is noted that two upper limits of $15\varepsilon_y$ and $C_1\varepsilon_u$ are placed on the CSM limiting strain (ε_{csm}) in the proposed CSM. Thus, Eqs. (24-25) were adopted to determine the moment resistances of hot-finished steel CHS and EHS with $\varepsilon_{csm}>\varepsilon_y$ in this study.

7. Assessment of design methods

Results of tubular beams obtained from tests in Section 4 and numerical simulations in Section 5 were used to assess the current codified design methods and the proposed CSM. The numerical and test moment capacities (M_u) were compared with moment resistances ($M_{u,pred}$) predicted by EN 1993-1-1 [1], EN 1993-1-5 [2], EN 1993-1-6 [5], ANSI/AISC 360-10 [3] and AISI S100 [4], the DSM [6, 7] and the proposed CSM. It is noted that design rules for EHS in bending are not available in current design codes and specifications [1-5], and thus the moment capacities obtained from design equations proposed by Chan and Gardner [29] ($M_{u,Chan}$) and the DSM ($M_{u,DSM}$) were compared with those determined by the proposed CSM ($M_{u,CSM}$). Partial factors in design equations were set to unity, and measured or modelled geometries material properties of tubular beams were used, in order to allow objective and direct comparison. Figs. 9-11 show the comparison of numerical and test moment resistances (M_u) normalised by predicted capacities ($M_{u,pred}$) of CHS, EHS, SHS and RHS beams, and results of statistical analysis of $M_u/M_{u,pred}$ ratios are summarised in Tables 11-13. The mean values of $M_u/M_{u,pred}$ for CHS determined by the Eurocode 3 [1, 5], ANSI/AISC 360-10 [3], AISI S100 [4], the DSM [6, 7] and the proposed CSM are 1.19, 1.13, 1.18, 1.29 and 1.03 with corresponding COV of 0.18, 0.13, 0.13, 0.19 and 0.12. The mean values of $M_u/M_{u,pred}$ for EHS calculated from the strength equations proposed by Chan and Gardner [29], the DSM [6, 7], and the proposed CSM are 1.19, 1.40 and 1.10 with corresponding COV of 0.12, 0.22 and 0.12. The mean values of $M_u/M_{u,pred}$ for SHS and RHS obtained from the Eurocode 3 [1, 2], ANSI/AISC 360-10 [3], AISI S100 [4], the DSM [6, 7] and the proposed CSM are 1.16, 1.15, 1.29, 1.33 and 1.07 with corresponding COV of 0.11, 0.11, 0.17, 0.15 and 0.08. It is noted that the current DSM [6, 7] is for the design of cold-formed structural steel members with flat elements and the adopted yield slenderness limit λ_p=0.776 (see Eq. (1)) is not suitable for CHS and EHS in this study (see Fig. 5). It is therefore concluded that the proposed CSM is capable of producing more accurate and less scattered capacity prediction for high strength steel CHS, EHS, SHS and RHS than the current design methods [1-7, 29].

8. Conclusions

This paper extends the scope of deformation-based continuous strength method (CSM) for the structural design of non-slender and slender high strength steel CHS, EHS, SHS and RHS under bending, covering

hot-finished and cold-formed steel tubular sections. Results of 146 existing tests in the literature were collated and a parametric study on 660 high strength steel tubular beams was conducted. Base curves and resistance functions were proposed for the tubular sections. Bi-linear and tri-linear material models were adopted for cold-formed and hot-finished steel tubular sections, respectively. The test and numerical results were used to evaluate the proposed CSM, the direct strength method (DSM) and design methods in EN 1993-1-1, EN 1993-1-5, EN 1993-1-6, ANSI/AISC 360-10 and AISI S100. The proposed CSM can provide more accurate and consistent prediction of moment capacities than the current DSM and codified design methods.

Acknowledgements

The authors appreciate the support from the Chinese National Engineering Research Centre for Steel Construction (Hong Kong Branch) at The Hong Kong Polytechnic University and the research seed funds from The Hong Kong Polytechnic University (PolyU/1-ZE50/G-YBUU). The first author is also grateful for the support given by the Research Grants Council of Hong Kong for the Hong Kong PhD Fellowship Scheme.

References

[1] EN 1993-1-1. Eurocode 3: Design of steel structures – Part 1.1: General rules and rules for buildings. Brussels: European Committee for Standardization (CEN); 2005.

[2] EN 1993-1-5. Eurocode 3: Design of steel structures – Part 1.5: Plated structural elements. Brussels: European Committee for Standardization (CEN); 2006.

[3] ANSI/AISC 360-10. Specification for structural steel buildings. Chicago: American Institute of Steel Construction (AISC); 2010.

[4] AISI S100. North American specification for the design of cold-formed steel structural members. Washington: American Iron and Steel Institute (AISI); 2016.

[5] EN 1993-1-6. Eurocode 3: Design of steel structures – Part 1.6: Strength and stability of shell structures. Brussels: European Committee for Standardization (CEN); 2007.

[6] Schafer BW, Peköz T. Direct strength predictions of cold-formed steel members using numerical elastic buckling solutions. In: Proceedings of the fourteenth international speciality conference on cold-formed steel structures. St. Louis (MO, USA); 1998.

[7] Schafer BW. Review: the direct strength method of cold-formed steel member design. J Construct Steel Res 2008; 64(7): 766–78.

[8] Gardner L, Nethercot D. Structural stainless steel design: a new approach. Struct Eng 2004; 82: 2-28.

[9] Yun X, Gardner L, Boissonnade N. The continuous strength method for the design of hot-rolled steel cross-sections. Eng Struct 2018; 157: 179-191.

[10] Yun X, Gardner L. The continuous strength method for the design of cold-formed steel non-slender tubular cross-sections. Eng Struct 2018; 175: 549-564.

[11] Gardner L. The continuous strength method. Proc ICE – Struct Build 2008;161 (3):127–33.

[12] Theofanous M, Propsert T, Knobloch M, Gardner L. The continuous strength method for steel cross-section design at elevated temperatures. Thin-Walled Struct 2016; 98: 94–102.

[13] Buchanan C, Gardner L, Liew A. The continuous strength method for the design of circular hollow sections. J Constr Steel Res 2016; 118:207–16.
[14] Saliba N G, Gardner L. Deformation-based design of stainless steel cross-sections in shear. Thin-Wall Struct 2018; 123: 324-332.
[15] Afshan S, Gardner L. The continuous strength method for structural stainless steel design. Thin-Walled Struct 2013;68: 42–49.
[16] Ahmed S, Ashraf M, Anwar-Us-Saadat M. The continuous strength method for slender stainless steel cross-sections. Thin-Walled Struct 2016; 107: 362–376.
[17] Zhao O, Afshan S, Gardner L. Structural response and continuous strength method design of slender stainless steel cross-sections. Eng Struct 2017; 140: 14–25.
[18] Su MN, Young B, Gardner L. The continuous strength method for the design of aluminium alloy structural elements. Eng Struct 2016; 122: 338–348.
[19] Lan XY, Chen JB, Chan TM, Young B. The continuous strength method for the design of high strength steel tubular sections in compression. Eng Struct 2018; 162: 177-187.
[20] Schafer BW, Ádány S. Buckling analysis of cold-formed steel members using CUFSM: conventional and constrained finite strip methods. In: Proceedings of the eighteenth international speciality conference on cold-formed steel structures. Orlando (USA); 2006.
[21] ABAQUS /Standard. Version 6.13-1. USA: K. a. S. Hibbit; 2013.
[22] Yun X, Gardner L. Stress-strain curves for hot-rolled steels. J Construct Steel Res 2017; 133: 36-46.
[23] Sedlacek G, Dahl W, Stranghöner N, Kalinowski B, Rondal J, Boeraeve P. Investigation of the rotation behaviour of hollow section beams. ECSC Research Project, Final Report, 7210/SA/119, 1995.
[24] Gresnigt A.M., L. van Foeken. Local buckling of UOE and seamless steel pipes. Proceedings of the Eleventh (2001) International Offshore and Polar Engineering Conference. J. Chung, L. Matsui, H. Moshagen (Eds.), 2001; 131–142 (Stavanger. ISBN 1880653516).
[25] Elchalakani M, Zhao XL, Grzebieta R. Bending tests to determine slenderness limits for cold-formed circular hollow sections. J Construct Steel Res 2002; 58: 1407-1430.
[26] Jiao H, Zhao XL. Section slenderness limits of very high strength circular steel tubes in bending. Thin-Walled Struct 2004; 42: 1257-1271.
[27] Elchalakani M, Zhao XL, Grzebieta R. Plastic slenderness limits for cold-formed circular hollow sections. Aust J Struct Eng; 2016; 3(3): 127-141.
[28] Ma JL, Chan TM, Young B. Experimental investigation of cold-formed high strength steel tubular beams. Eng Struct 2016; 126: 200-209.
[29] Chan TM, Gardner L. Bending strength of hot-rolled elliptical hollow sections. J Construct Steel Res 2008; 64: 971-986.
[30] Wilkinson T, Hancock GJ. Tests to examine compact web slenderness of cold-formed RHS. J Struct Eng (ASCE) 1998; 124(10): 1166-1174.

[31] Wang J, Afshan S, Gkantou M, Theofanous M, Baniotopoulos C, Gardner L. Flexural behaviour of hot-finished high strength steel square and rectangular hollow sections. J Constr Steel Res, 2016; 121: 97-109.

[32] Ma JL, Chan TM, Young B. Design of cold-formed high strength steel tubular beams. Eng Struct 2017; 151: 432-443.

[33] Ma JL, Chan TM, Young B. Material properties and residual stresses of cold-formed high strength steel hollow sections. J Construct Steel Res 2015; 109:152-65.

[34] EN 10210-2. Hot finished structural hollow sections of non-alloy and fine grain steels-Part 2: Tolerances, dimensions and sectional properties. Brussels: European Committee for Standardization (CEN); 2006.

[35] EN 10219-2. Cold formed structural hollow sections of non-alloy and fine grainsteels-Part 2: Tolerances, dimensions and sectional properties. Brussels: European Committee for Standardization (CEN); 2006.

[36] Liew A, Gardner L, Block P. Moment-Curvature-Thrust Relationships for Beam-Columns. Struct 2017; 11: 146-154.

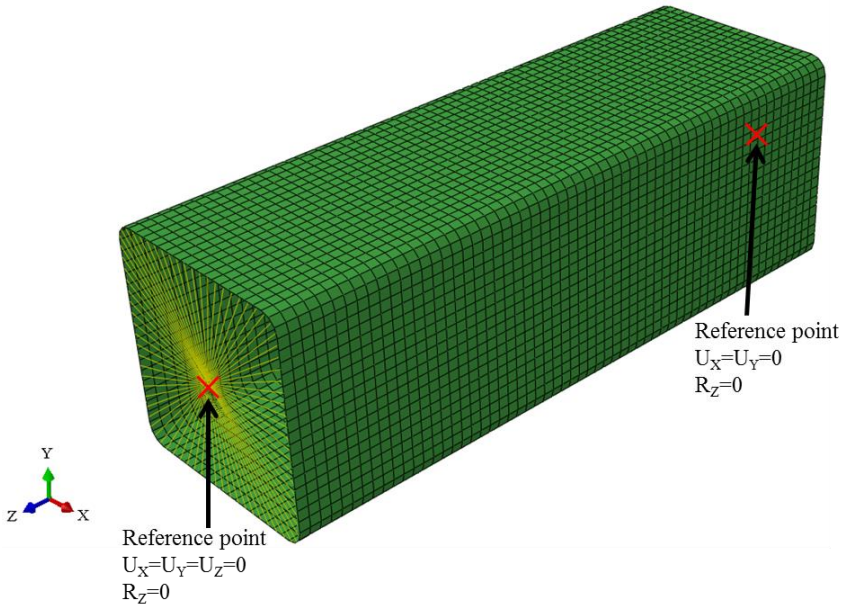

Fig. 1. Boundary conditions adopted in pure bending model.

(a) S133×4-B [28]

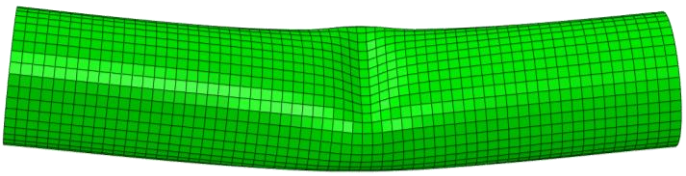

(b) FEA-CHS

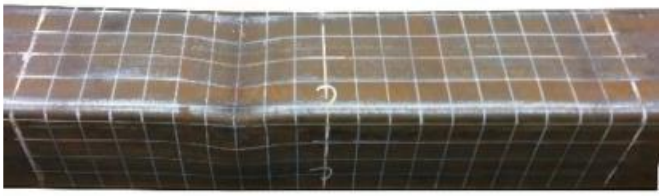

(c) H140×140×5-B [28]

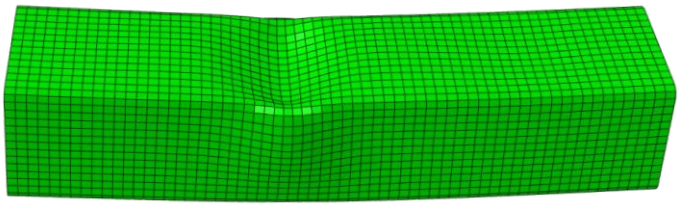

(d) FEA-SHS

Fig. 2. Comparison of failure modes observed in tests with those predicted by FE analysis.

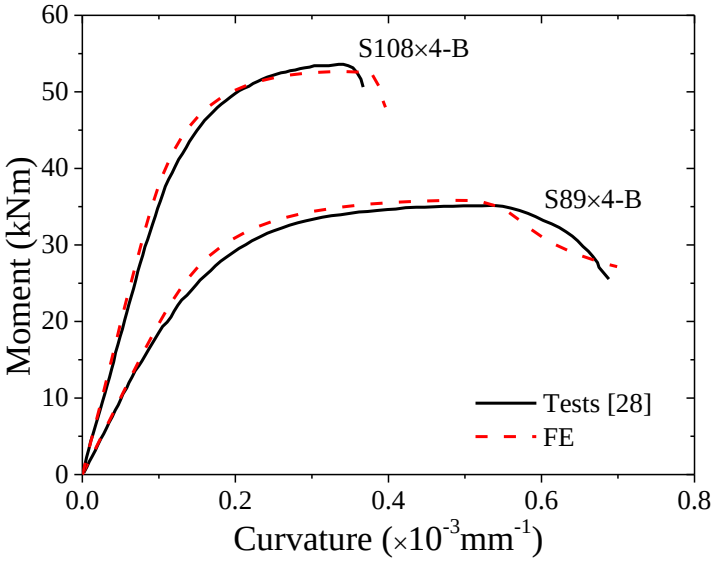

(a) CHS

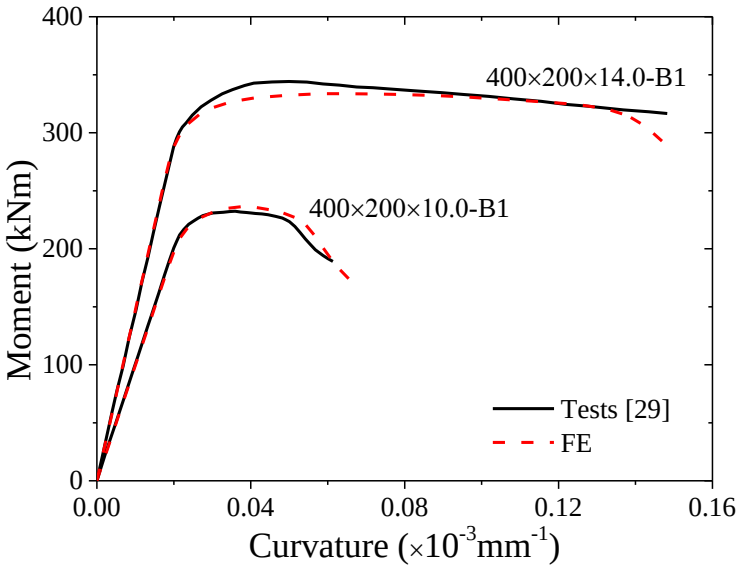

(b) EHS

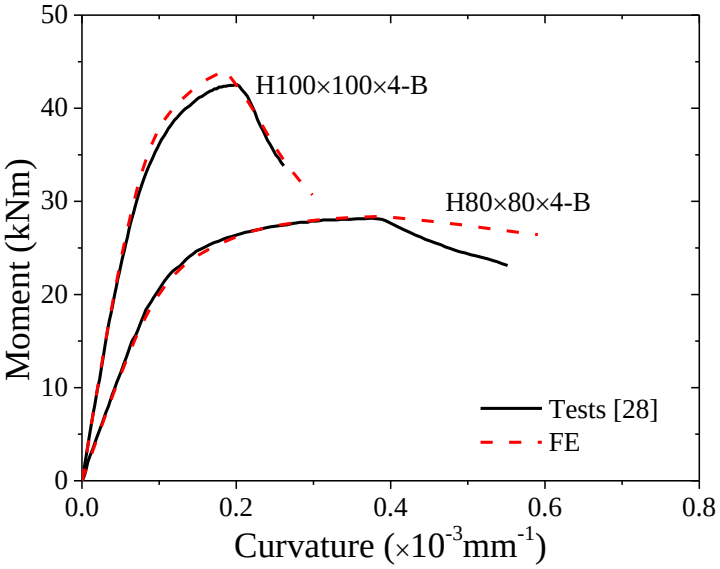

(c) SHS and RHS

Fig. 3. Comparison of moment-curvature curves.

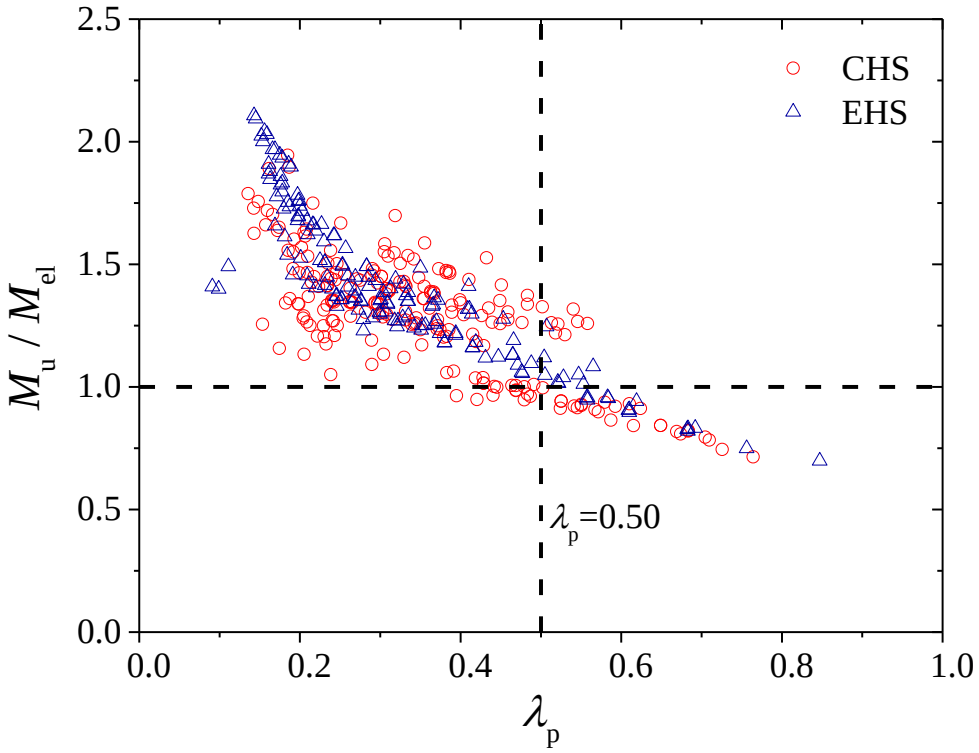

(a) CHS and EHS

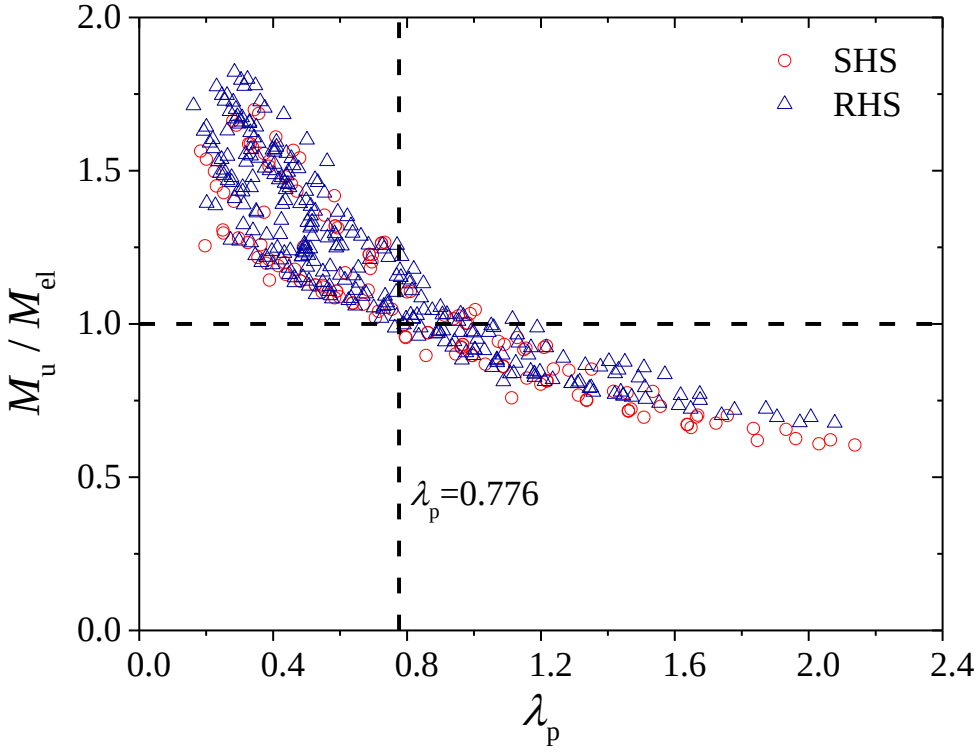

(b) SHS and RHS

Fig. 4. Ultimate capacity normalised by elastic moment resistance of tubular beams.

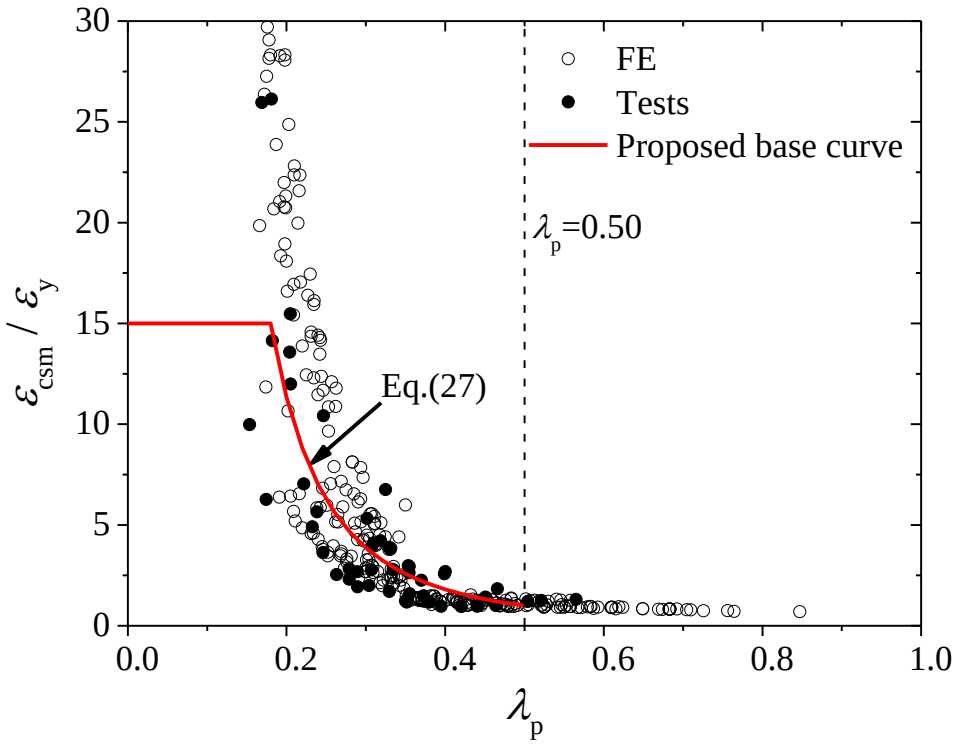

(a) Non-slender cross-sections

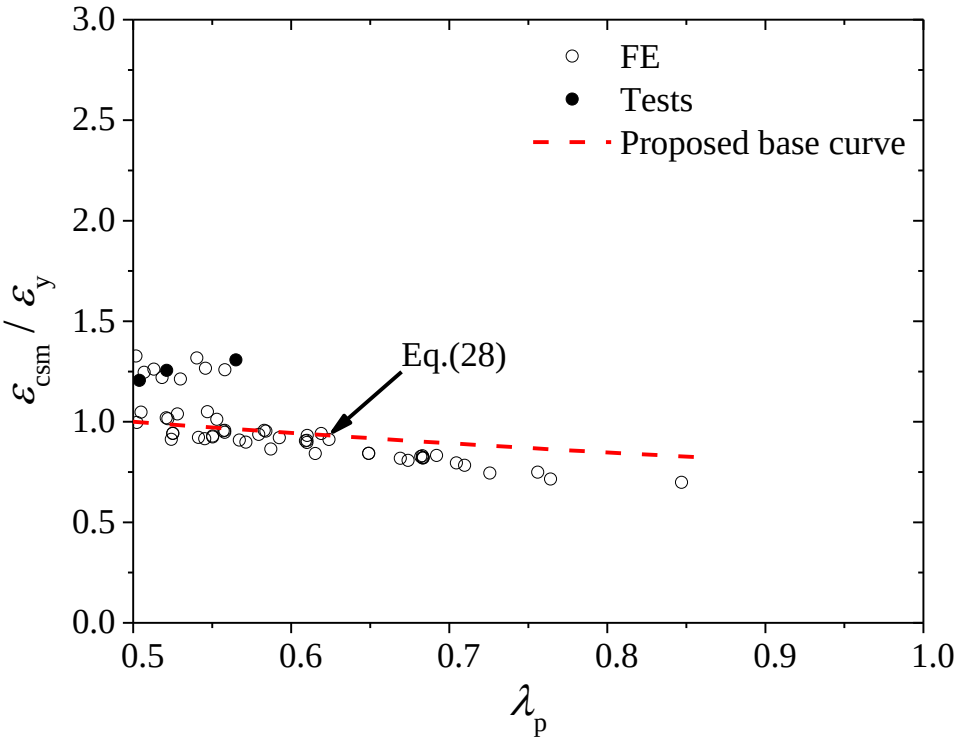

(b) Slender cross-sections

Fig. 5. Base curves for CHS and EHS with test and numerical data.

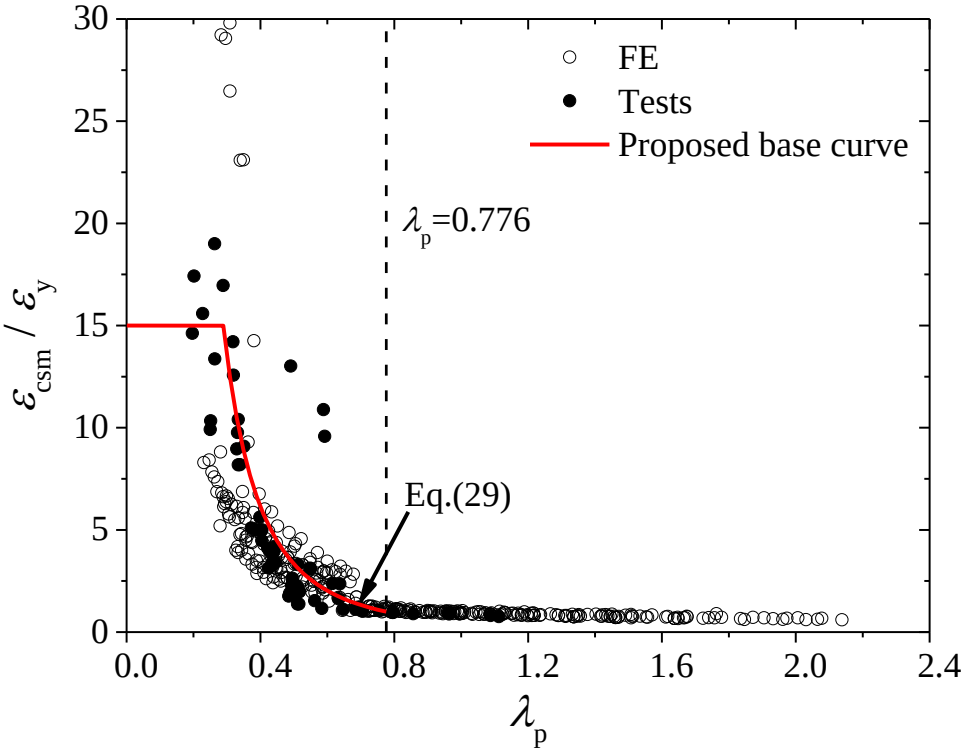

(a) Non-slender cross-sections

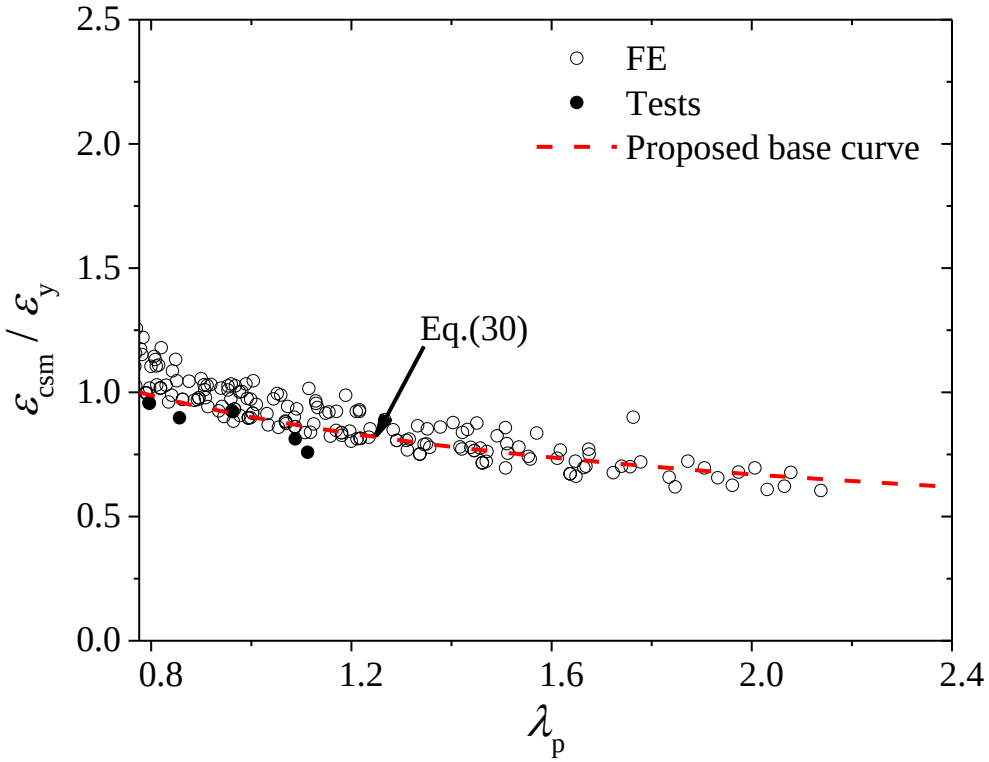

(b) Slender cross-sections

Fig. 6. Base curves for SHS and RHS with test and numerical data.

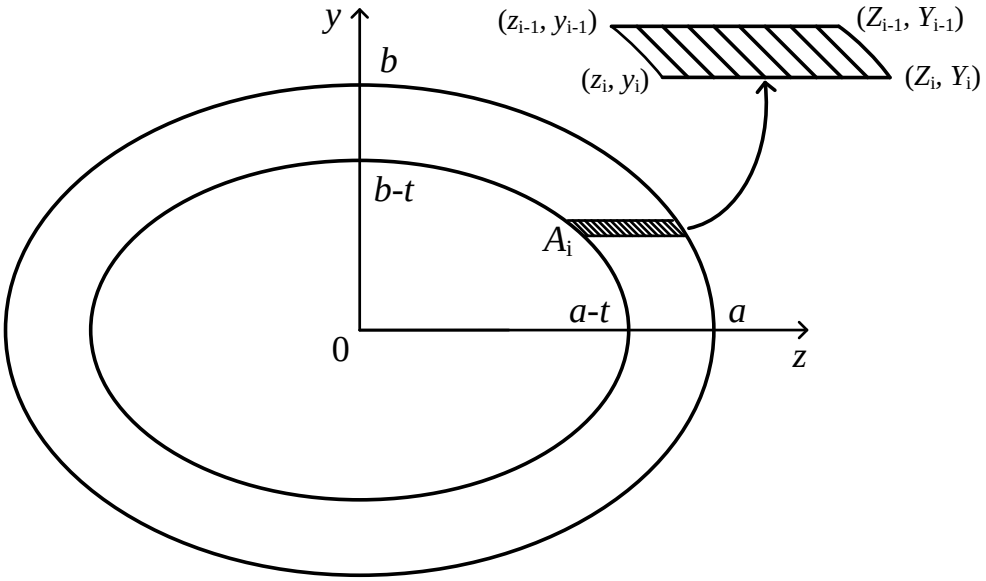

Fig. 7. Discretisation of an elliptical hollow section.

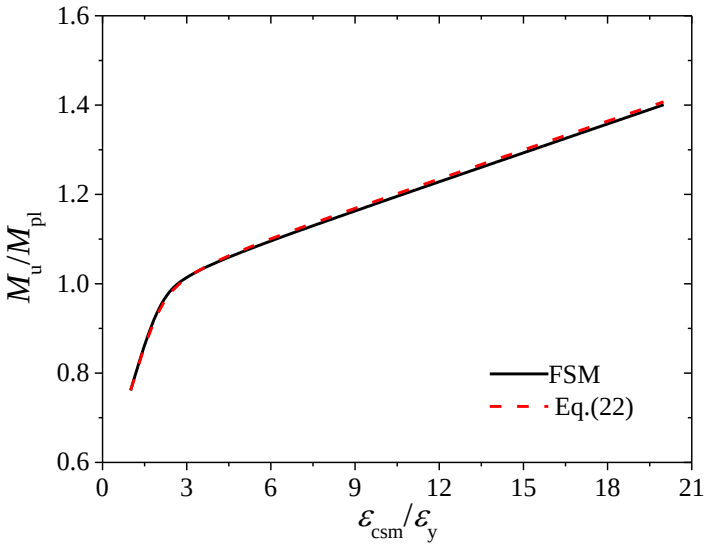

(a) Cold-formed steel CHS

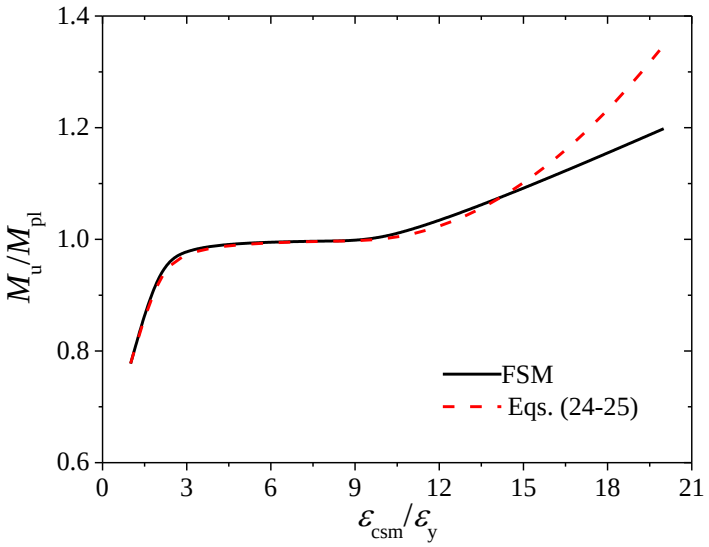

(b) Hot-finished steel CHS

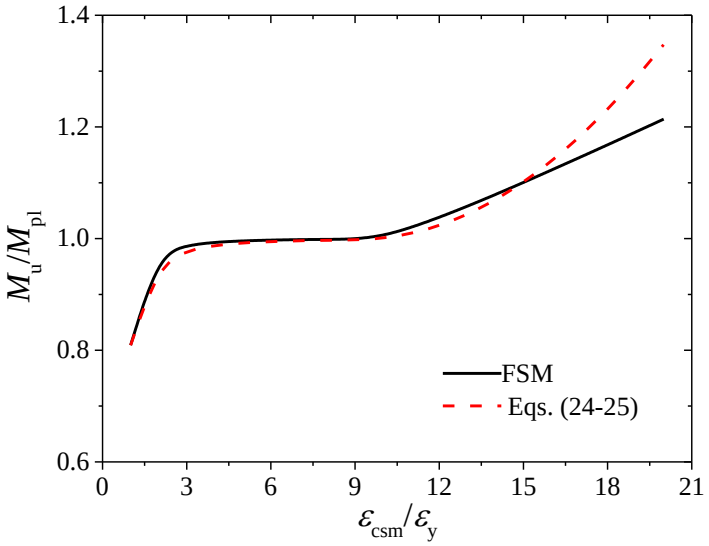

(c) Hot-finished steel EHS

Fig. 8. Comparison of moment capacities obtained from the FSM with CSM predictions.

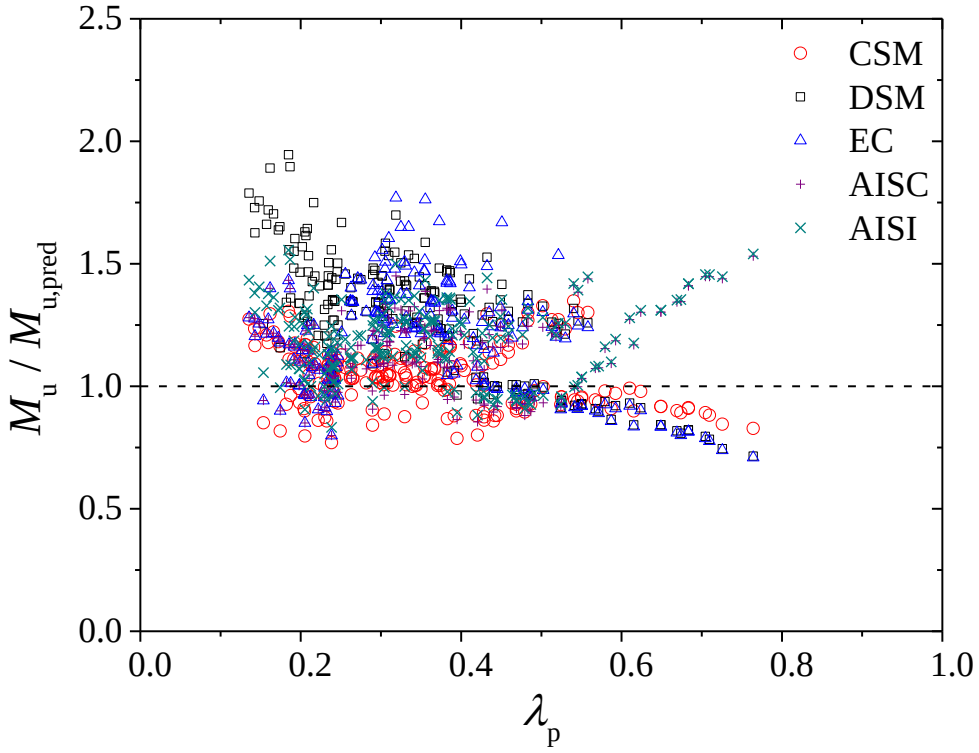

Fig. 9. Comparison of test and numerical capacities of 215 CHS beams with predicted resistances.

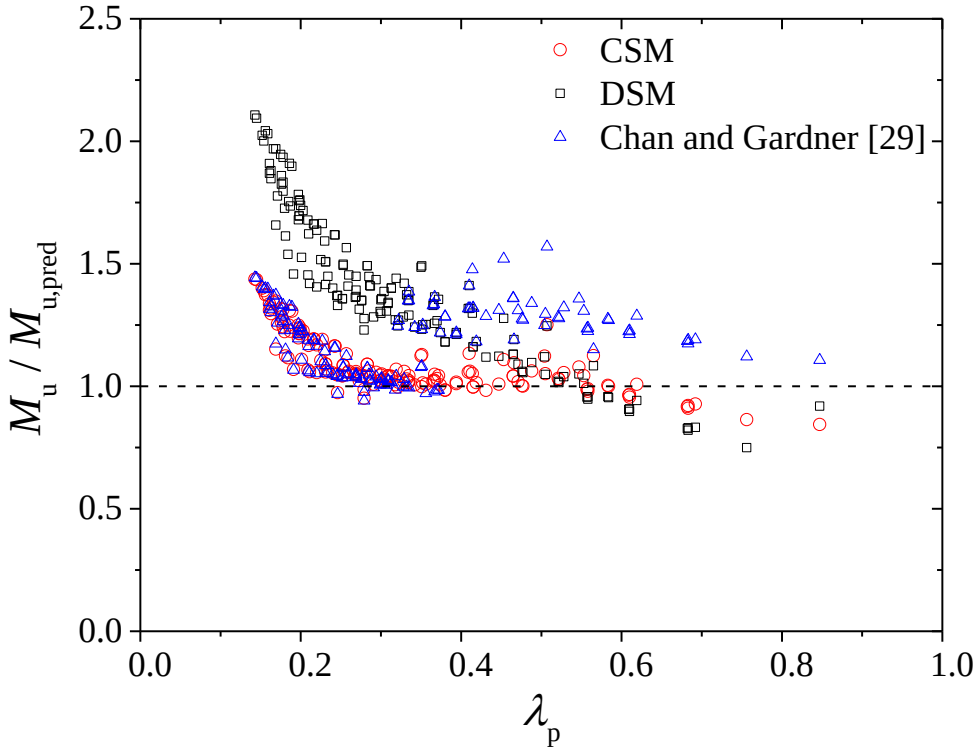

Fig. 10. Comparison of test and numerical capacities of 160 EHS beams with predicted resistances.

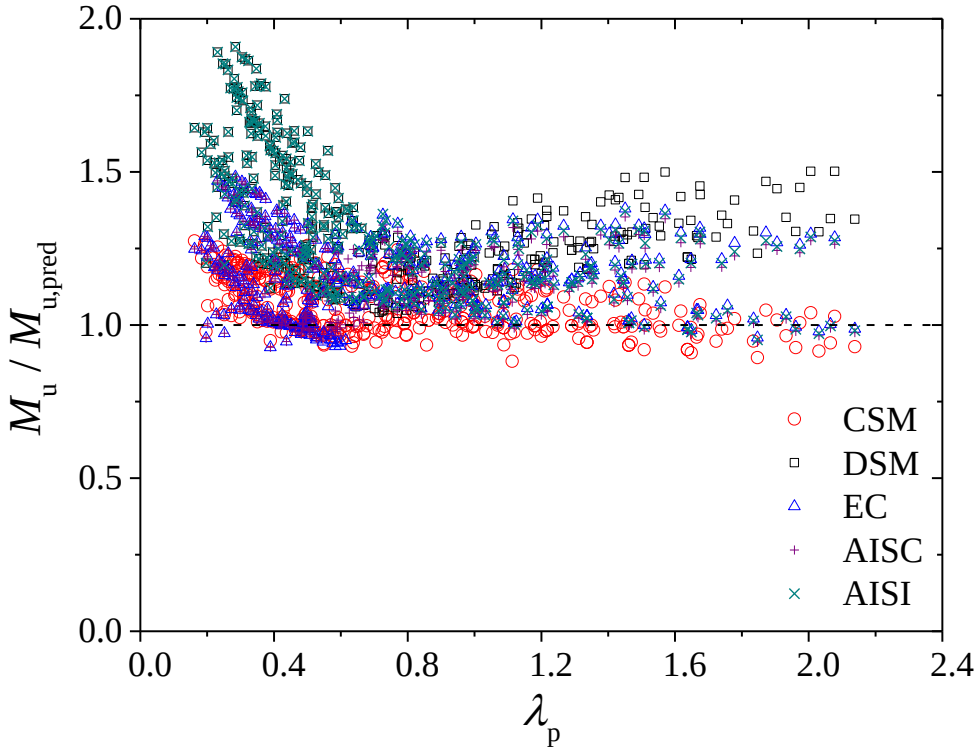

Fig. 11. Comparison of test and numerical capacities of 431 SHS and RHS beams with predicted resistances.

Table 1

Coefficients for the CSM bi-linear material models (Buchanan et al. [13]).

Steel type	C_1	C_2	C_3	C_4
Very high strength steel	0.40	0.45	0.60	0
Cold-formed steel	0.40	0.45	0.60	0
Austenitic and duplex stainless steel	0.10	0.16	1.00	0
Ferritic stainless steel	0.40	0.45	0.60	0
Aluminium	0.50	0.50	0.13	0.06

Table 2

Experimental tests on CHS beams.

Reference	f_y (MPa)	Fabrication method	λ_p	No. of tests
Sedlacek et al. [23]	269-564	Hot-finished	0.16-0.30	23
Gresnigt and Foeken [24]	450-479	Cold-formed	0.20-0.29	4
Elchalakani et al. [25]	365-412	Cold-formed	0.24-0.46	12
Jiao and Zhan [26]	1284-1398	Cold-formed	0.30-0.52	8
Elchalakani et al. [27]	469-568	Cold-formed	0.15-0.25	9
Ma et al. [28]	1014-1180	Cold-formed	0.31-0.40	9
Total			0.15-0.52	65

Table 3

Experimental tests on EHS beams.

Reference	f_y (MPa)	Fabrication method	λ_p	No. of tests
Chan and Gardner [29]	377-434	Hot-finished	0.18-0.56	10

Table 4

Experimental tests on SHS and RHS beams.

Reference	f_y (MPa)	Fabrication method	λ_p	No. of tests
Ma et al. [28]	663-1005	Cold-formed	0.32-1.01	16
Wilkinson and Hancock [30]	349-457	Cold-formed	0.29-0.70	44
Wang et al. [31]	497-789	Hot-finished	0.16-0.49	11
Total			0.16-1.01	71

Table 5

Comparison of numerical results with test data of CHS beams [28].

Specimen	D (mm)	t (mm)	ω_0 (mm)	f_y (MPa)	k_u (mm^{-1})	M_u (kN)	k_{FE}/k_u	M_{FE}/M_u
V89×3-B	88.8	2.96	0.174	1054	0.00038	23.8	0.92	0.98
V89×3-B#	89	2.95	0.174	1054	0.00034	23.8	1.00	0.98
V89×4-B	89	3.9	0.132	1053	0.00049	30.9	0.94	0.99
S89×4-B	88.9	3.86	0.072	1180	0.00054	35.1	0.88	1.01
S89×4-B#	89	3.9	0.116	1180	0.00055	35.9	0.90	1.00
S108×4-B	108.2	3.9	0.141	1180	0.00034	53.6	1.01	0.98
S133×4-B	133.4	3.93	0.173	1159	0.00025	79	1.10	1.00
S133×4-B#	133.4	3.91	0.174	1159	0.00026	77.9	1.00	1.01
S139×6-B	139.4	5.93	0.168	1014	0.00035	137.1	0.91	0.98
Mean							0.96	0.99
COV							0.07	0.01

Table 6

Comparison of numerical results with test data of EHS beams [29].

Specimen	Axis of bending	$2a$ (mm)	$2b$ (mm)	t (mm)	ω_0 (mm)	f_y (MPa)	k_u (mm^{-1})	M_u (kN)	k_{FE}/k_u	M_{FE}/M_u
400×200×8.0-B1	Minor	396.09	207.63	7.75	0.430	429.0	0.000024	186	1.10	1.09
400×200×10.0-B1	Minor	396.06	207.54	9.65	0.140	401.0	0.000036	232	1.07	1.05
400×200×12.5-B1	Minor	401.54	201.01	12.13	2.920	395.0	0.000041	288	1.15	1.05
400×200×14.0-B1	Minor	400.32	200.04	14.48	3.690	397.5	0.000050	343	1.24	0.97
400×200×16.0-B1a	Minor	403.16	201.08	15.63	0.570	378.5	0.000048	331	1.32	1.05
500×250×8.0-B1	Minor	495.34	255.85	7.78	2.010	413.0	0.000017	291	1.11	0.95
500×250×8.0-B2	Major	491.74	260.92	7.78	0.470	413.0	0.000027	497	1.39	1.01
Mean									1.20	1.02
COV									0.10	0.05

Table 7

Comparison of numerical results with test data of SHS and RHS beams [28].

Specimen	H (mm)	B (mm)	t (mm)	ω_0 (mm)	f_{yf} (MPa)	f_{yc} (MPa)	k_u (mm^{-1})	M_u (kN)	k_{FE}/k_u	M_{FE}/M_u
H80×80×4-B	80.1	80.3	3.92	0.172	792	933	0.00038	28.2	1.00	1.01
H80×80×4-B#	80.1	80.2	3.93	0.172	792	933	0.00038	28.1	1.01	1.01
H100×100×4-B	100.4	100.3	3.94	0.253	735	931	0.00019	42.5	0.95	1.03
H120×120×4-B	121.4	121	3.95	0.162	689	923	0.00011	56.1	1.05	1.04
H140×140×5-B	140.3	141.3	4.94	0.280	708	912	0.00011	97.6	0.94	1.03
H140×140×5-B#	140.5	141.2	4.95	0.280	708	912	0.00011	97.6	0.94	1.03
H140×140×6-B	141.2	140.9	5.98	0.230	663	958	0.00017	121.7	0.93	1.04
H160×160×4-B	160.5	160.6	3.99	0.654	744	910	0.00007	84.4	0.97	1.01
H100×50×4-B	100.3	50.3	3.93	0.251	724	859	0.00046	16.9	0.86	1.06
H50×100×4-B	50.3	100.2	3.97	0.251	724	859	0.00079	30.9	0.87	1.08
H200×120×5-B	200.4	121.5	4.95	0.420	738	895	0.00008	90.3	1.05	1.03
H120×200×5-B	121.2	200.4	4.95	0.420	738	895	0.00009	157.0	0.98	1.07
V80×80×4-B	80.2	80.3	3.95	0.214	1005	1187	0.00039	37.5	0.87	0.85
V100×100×4-B	100.2	100.2	3.96	0.284	978	1114	0.00020	50.9	0.73	1.09
V120×120×4-B	121.1	120.9	3.93	0.394	960	1114	0.00012	68.6	0.94	1.05
V120×120×4-B#	121.1	120.9	3.91	0.394	960	1114	0.00013	68.5	0.91	1.05
Mean									0.94	1.03
COV									0.09	0.05

Table 8

Parameters of hot-finished and cold-formed high strength steel beams of CHS, EHS, SHS and RHS.

Cross-section	D (mm)	$2a \times 2b$ (mm)	$H \times B$ (mm)	t (mm)	λ_p
CHS-HF	101.6	-	-	1, 2, 3.2, 5, 10	0.14-0.59
	219.1	-	-	2, 4, 5, 10, 16	
	323.9	-	-	3, 4, 5, 10, 16	
	406.4	-	-	4, 6, 8, 12.5, 16	
	508.0	-	-	4, 6, 8, 12.5, 16	
CHS-CF	101.6	-	-	1, 2, 3.2, 5, 10	0.17-0.76
	219.1	-	-	2, 4, 5, 10, 16	
	323.9	-	-	3, 4, 5, 10, 16	
	406.4	-	-	4, 6, 8, 12.5, 16	
	508.0	-	-	4, 6, 8, 12.5, 16	
EHS-HF	-	150×75	-	1, 2, 4, 6.3, 10	0.14-0.85
	-	200×100	-	2, 4, 6.3, 8, 12.5	
	-	250×125	-	3, 4, 6, 10, 12.5	
	-	300×150	-	3, 4, 8, 12.5, 16	
	-	400×200	-	4, 6, 8, 12, 14	
SHS-HF	-	-	100×100	1.5, 2, 4, 6.3, 10	0.18-1.85
	-	-	200×200	3, 4, 5, 10, 16	
	-	-	300×300	4, 5, 6.3, 10, 16	
	-	-	400×400	6, 8, 10, 14.2, 16	
SHS-CF	-	-	100×100	1.6, 3, 5, 6, 8	0.28-2.14
	-	-	200×200	2.9, 5, 8, 12, 15	
	-	-	300×300	4.5, 6, 8, 12, 20	
	-	-	400×400	7, 9, 10, 12, 16	
RHS-HF	-	-	150×100	2.5, 3, 4, 6.3, 10	0.19-1.74
	-	-	200×100	2.9, 3.5, 4, 8, 10	
	-	-	300×200	4.5, 5, 5.5, 10, 16	
	-	-	400×200	5.5, 6.3, 10, 14.2, 16	
RHS-CF	-	-	150×100	4, 6, 8, 9.4, 10	0.23-2.08
	-	-	200×100	3.4, 3.8, 4.1, 8.8, 9.4	
	-	-	300×200	6, 6.4, 7.5, 15, 17.6	
	-	-	400×200	5.8, 6, 6.4, 11, 14	

Table 9

Material parameters for hot-finished high strength steel beams of CHS, EHS, SHS and RHS (Lan et al. [19]).

Steel grade	E (GPa)	f_y (MPa)	f_u (MPa)	ε_u (%)
S460	210	460	550	9.82
S550	210	550	640	8.44
S690	210	690	770	6.23

Table 10

Material parameters for cold-formed high strength steel beams of CHS, SHS and RHS (Ma et al. [33]).

Steel grade	CHS				Flat portion of SHS and RHS				Corner portion of SHS and RHS			
	E (GPa)	f_y (MPa)	f_u (MPa)	ε_u (%)	E (GPa)	f_y (MPa)	f_u (MPa)	ε_u (%)	E (GPa)	f_y (MPa)	f_u (MPa)	ε_u (%)
S700	214	772	816	4.64	212	719	840	4.28	212	897	983	1.63
S900	210	1054	1116	2.26	208	982	1149	2.08	209	1138	1245	2.17
S1100	207	1152	1317	2.20	205	1073	1356	2.03	206	1245	1470	2.12

Table 11

Statistical analysis for 215 CHS beams.

	M_u / $M_{u,EC3}$	M_u / $M_{u,AISC}$	M_u / $M_{u,AISI}$	M_u / $M_{u,DSM}$	M_u / $M_{u,CSM}$
Mean	1.19	1.13	1.18	1.29	1.03
COV	0.18	0.13	0.13	0.19	0.12

Table 12

Statistical analysis for 160 EHS beams.

	M_u / $M_{u,Chan}$	M_u / $M_{u,DSM}$	M_u / $M_{u,CSM}$
Mean	1.19	1.40	1.10
COV	0.12	0.22	0.12

Table 13

Statistical analysis for 431 SHS and RHS beams.

	M_u / $M_{u,EC3}$	M_u / $M_{u,AISC}$	M_u / $M_{u,AISI}$	M_u / $M_{u,DSM}$	M_u / $M_{u,CSM}$
Mean	1.16	1.15	1.29	1.33	1.07
COV	0.11	0.11	0.17	0.15	0.08